Ultrafast laser ablation of gold in liquids: Effect of laser pulse overlap-induced surface porosity on size distribution of formed nanoparticles

D.S. Ivanov, P. Shakhov, G. Tikhonowsky, A.A. Popov, A.N. Mayorov, I.N. Zavestovskaya, S.M. Klimentov, A.V. Kabashin

DOI: APSUSC-D-23-08280

Article type: regular

Ultrafast laser ablation of gold in liquids: effect of laser pulse overlap-induced surface porosity on size distribution of formed nanoparticles

D. S. Ivanov[a]*, P. Shakhov[b], G. Tikhonowsky[b], A. A. Popov[b], A. N. Mayorov[b], I. N. Zavestovskaya[a,b], S. M. Klimentov[b], and A.V. Kabashin[c]*

[a] Lebedev Physical Institute of the Russian Acad. Sci., Leninskiy Pr. 53, 119991 Moscow, Russia
[b] National Research Nuclear University "MEPhI", Institute of Engineering Physics for Biomedicine (PhysBio), Kashirskoe sh. 31, 115409 Moscow, Russia
[c]Aix-Marseille Université, CNRS, LP3, 163 Avenue de Luminy, 13288 Marseille, France

Highlights :

- Nanoparticles (NP) with demanded properties can be produced due to Pulsed Laser Ablation in Liquids (PLAL).
- There are two main mechanisms of NPs production that are sensitive to irradiation conditions.
- There are such laser processing regimes that allow for manipulation with the mechanisms of laser ablation.
- Activation of the appropriate mechanism of PLAL allows for formation of NPs with controllable size characteristics.

*To whom the correspondence should be addressed: ivanov@uni-kassel.de; andrei.kabashin@univ-amu.fr

Graphical abstract

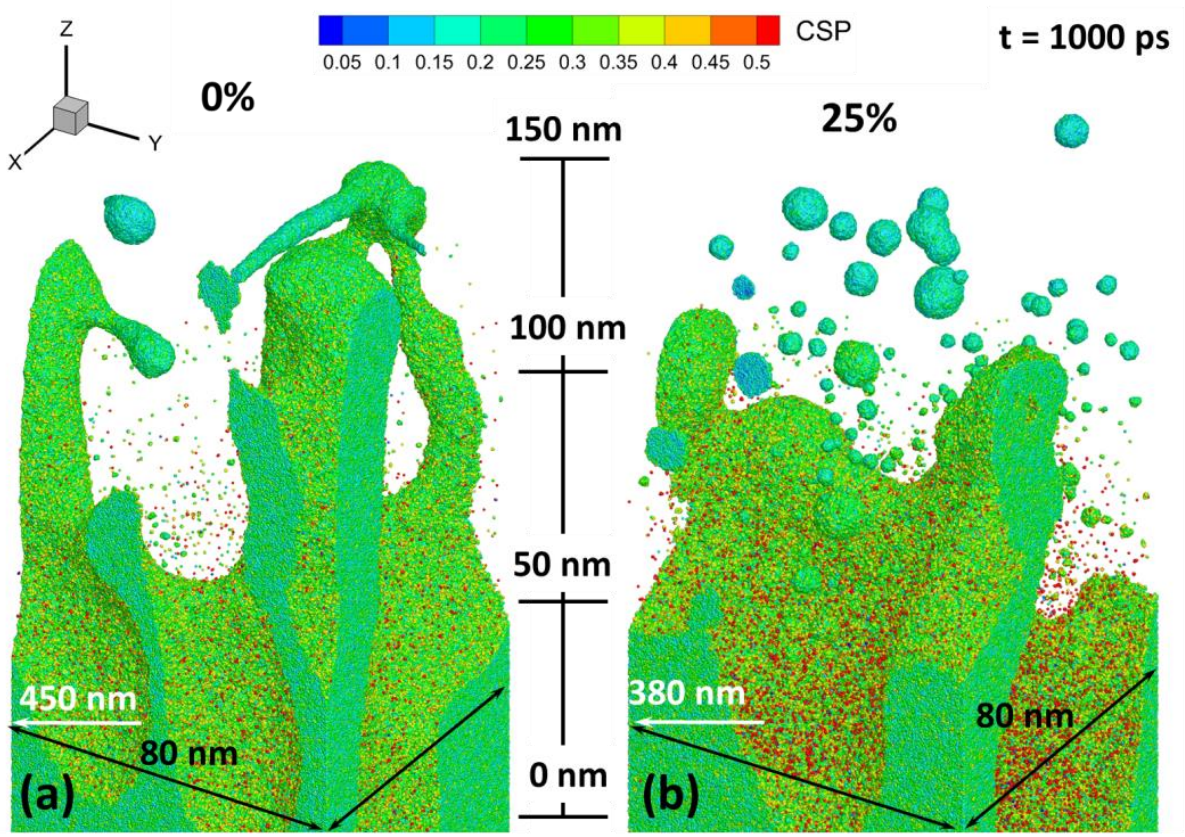

Abstract

Pulsed Laser Ablation in Liquids (PLAL) manifested itself as a powerful tool for the synthesis of nanoparticles (NPs) from a variety of materials of high demand in biomedicine. The mechanisms and regimes of nanostructures formation, however, still require clarification in order to better control the final NPs characteristics. Here, we present a numerical study of femtosecond laser-ablative production of metal (gold) NPs in water ambient using an advanced atomistic continuum approach, combining the Molecular Dynamics (MD) and Two Temperature Model into the frames of a single MD-TTM computational method. The model describes non-equilibrium laser-induced phase transitions at atomic level and accounts for the effect of free carriers in continuum. With the MD-TTM model we investigated the effect of slight porosity arising due to a partial overlap of laser craters during the scanning of laser beam over the target surface under a high repetition rate of laser pulses. For that purpose, we perform a simulation of 270 fs laser pulse interaction with solid and porous gold targets at the incident fluence of 2.5 J/cm^2. The obtained results revealed the manifestation of different regimes of ablation and different yield of the obtained NPs. The simulation results are compared with the corresponding experimental data. We found that depending on the scanning speed the ablation can follow thermal and spallation mechanisms of the material ejection, which are responsible for the appearance of fine and course populations of NPs correspondingly. In the case of clean target's surface ablation, when at high scanning speed of 3840 mm/s each pulse hits a fresh area, the material ejection is governed by both mechanisms, which leads to the appearance of bimodal population of NPs. Alternatively, a moderate scanning speed of 840 mm/s results in a partial overlap of the sequential laser spots on the surface and generated slight porosity removes the accumulation of laser-induced stresses. The spallation mechanism of the material ejection is therefore suppressed, which results in generation of a monomodal fine population of NPs with a 20 times larger yield. The obtained data are of importance to predict and control size characteristics of laser-synthesized nanomaterials.

Keywords

Pulsed laser ablation in liquids, Nanoparticles, Size distribution, Molecular Dynamics (MD), Two Temperature Model (TTM), atomistic-continuum model MD-TTM

1. Introduction

The role of nanoparticles (NPs) has become extremely important for the last two decades, as they can exhibit a series of unique properties that make them useful for a plethora of applications, including catalysis, photovoltaics, and biomedicine. The process of their manufacturing, however, remains challenging, as projected applications may impose severe requirements on physical and physico-chemical parameters of NPs. As an example, applications of NPs in biomedicine (bioimaging, therapeutics, targeted delivery of drugs) frequently require their parameters such as shape, mean size (usually in the range of 10 - 100s nm), and size distribution to be quite specific [1,2,3,4]. Such requirements are caused by the necessity of maximizing imaging or therapeutic functionality, and subsequent elimination of the NPs without any side effects [5,6]. The controllable size of NPs with low size dispersion becomes especially important in some tasks of diagnosis and treatment of cancers, e.g. in methods implying the use of NPs as sensitizers of magnetic field-induced [7] or photon-induced [8,9]local overheating (hyperthermia) of cancer cells leading to their death.

Methods of pulsed laser ablation are now increasingly popular for the synthesis of various nanomaterials (metallic, semiconductor, composite, etc.) [10, 11] presenting the main alternative to conventional chemical synthesis. This method is based on a natural production of nanoclusters during the interaction of powerful pulsed laser radiation with a solid target of virtually any material [12,13], which can then be released to a gaseous or liquid medium to form a nanostructured thin film [14,15,16,17] or a colloidal nanoparticle (NP) solution [18,19,20,21], respectively. Pulsed laser ablation in liquids (PLAL) has gained particular attention for last years (for review, see [11]). Since PLAL procedure does not require the use of specific chemical products and conditions, they are free of limitations of colloidal chemistry and can provide nanomaterials of controllable geometry and composition, which can be used in a variety of important applications, including biomedicine [22, 23, 24, 25], catalysis [26,27,28,29], photovoltaics [30].

Femtosecond laser ablation has demonstrated its especially high efficiency in the control of NPs size and composition in the absence of ligands [21,31]. One of advantages of this technique is related to a much lower energy per laser pulse needed to initiate ablation from a target. This leads to a drastic minimization of plasma and cavitation bubble effects, which are considered as important factors leading to uncontrollable growth of nanoclusters and related broadening of size dispersion [21,32]. As we recently showed, this technique makes possible a fine control

NPs size parameters for a variety of nanomaterials, including metal/semimetal [33,34,35] and semiconductor [36,37,38] NPs. However, some properties of femtosecond laser ablation are still not fully understood. One of such properties is related to a possible appearance of bimodal size distributions of laser-ablated metal NPs (Au, Ag) associated with the presence of finer (smaller size and lower dispersion) and coarser (larger and more size-dispersed) populations [21,31,32], although the second coarser population could be discriminated by a proper selection of laser parameters [21,32, 39]. It should be noted that the presence of such a bimodal distribution was equally reported for both short and long laser pulse durations and for a variety of metal and semiconductor materials (see e.g. [40,41,42,43,44,45]) suggesting common mechanisms for its origin.

An adequate theoretical description is still needed to identify all possible factors and mechanisms affecting size characteristics of NPs under different parameters of laser radiation and geometry of ablation. Here, approaches based on Molecular Dynamics (MD) have demonstrated the highest potential in the description of the very first stage of laser-matter interaction (within a few ns) characterized by a non-equilibrium processes of radiation energy deposition and the establishment of initial excited system parameters, which then determine the further evolution of diffusion, nucleation, coalescence and nanoparticle aggregation processes during subsequent plasma development and cavitation bubble stages [46].

Because the above-mentioned processes arise on a wide spatial and temporal scales, the classical MD methods cannot provide a complete description of the process and the final model should yet be complemented by methods describing the evolution of the excited electronic system and the nanoparticles growth during later stages. However, the suggested in this work atomistic-continuum approach could help one to identify some key factors affecting NPs size characteristics, and even give clear indications on possible mechanisms of NPs generation. In particular, it was proposed that the coarser population of the NPs could originate from the decompositions of Rayleigh-Taylor instabilities across the metal-liquid interface, whereas the finer one could appear due to an explosive boiling ablation mechanism and subsequent nucleation of the metallic vapor atoms into small coalescing clusters as a result of an intensive cooling process [47, 48, 49,50]. It was also noted in [51,52] that both the growth of Rayleigh-Taylor instabilities and the generation of significant amount of vapor can be attributed to different regimes of the laser energy deposition: mechanical confinement and thermal confinement [53]. While most of the experimental conditions are accompanied by both regimes, the former one is responsible for the accumulation of strong compressive stresses inside the

target due to fast and deep heating. These stresses then pass through a relaxation stage via a strong recoil of pressure waves, followed by the establishment of a hydrodynamic motion in the molten part of the material, on the surface of which the Rayleigh-Taylor instabilities are generated. The latter one (thermal confinement regime) results in a significant elevation of target's surface temperature and a subsequent removal of material via the explosive boiling mechanism [54]. If so, by means of variation of the laser irradiation parameters it becomes possible to suppress or isolate one or another regime of the target's heating in order to control the final populations of generated NPs. In particular, as it was found in [39,50,52], long pulses (with the duration much longer than the characteristic *e-ph* equilibration time ~ 1 - 30 ps) lead to a gradual relaxation of any developed stresses induced in the target (typical for ultrashort pulses) and if the applied fluence does not lead to a significant elevation of electronic temperature (where electron conductivity is high [55,56]), the heat is mainly confined in the proximity of the surface. The material ejection in such a case follows the explosive boiling mechanism leading to the formation of the finer NPs population. These finding are consistent with recent observations found in other theoretical works [49,50,57,58].

We believe that the mechanisms of nanoparticle formation under PLAL can be better understood if one clearly identifies and discriminates different factors, which can affect the NPs growth. One of such factors is related to a possible appearance of porosity in the upper layer of the target surface under its multi-pulse ablation. Recent experiments on NPs generation due to PLAL in the multi-pulse regime revealed the formation of unimodal size distribution if the irradiated sample possesses a predeveloped porosity [46]. Indeed, such a porosity can appear at the periphery of laser spots while a laser beam is scanned over the target surface. As it was shown in [59], the applied fluence in the periphery of the laser spots can be just below the ablation threshold value, which can lead to the formation of subsurface voids (with vacuum inside) under the irradiated area without the actual ablation phenomenon (material removal via spallation mechanism) [49,60,61,62,63]. Here, for a certain scanning speed, the overlap can be partial, which is supposed to lead to a minor porosity, but even this porosity level could change the ablation threshold and material removal mechanisms compared to the ablation from a fresh (undamaged) surface. On the other hand, smaller scanning speeds can lead to a significant overlap yielding the formation of trenches with spike-like surface relieves, which also changes its thermophysical properties and affects the ablation process to alter specifications of the obtained NPs (shape, mean size, and size distribution).

Since during the first stage of laser-material interaction the formed porosity is supposed to strongly affect the process of laser energy deposition and its subsequent dissipation during the second stage, we believe that methods of MD-based modeling might offer an efficient tool to describe such an effect on the ablation process and explain size characteristics of formed NPs. Here, we carry out large-scale MD-based simulations to consider the effect of laser-induced target's porosity during the interaction of fs laser radiation with a gold target in water. Due to a complicated experimental evaluation of the laser-induced porosity, in this work we investigate only its qualitative effects. We show that depending on the absence or presence of this subsurface porosity, the dissipation of the deposited laser energy can follow different channels, which results in the appearance of either bimodal or monomodal size distributions of formed NPs. In particular, in our simulations we are targeting the NPs generation of 10nm +/- 2nm for, which are suitable for many applications, including biomedicine and catalysis.

2. Methods

2.1 Experimental methods

Gold (Au) NPs were obtained by femtosecond laser ablation in deionized water. A gold target and a glass vessel (14x28x40 mm) were initially cleaned in an ultrasonic bath for 5 minutes. A beam (60 μm diameter) from a Yb: KGW laser (1030 nm wavelength, 270 fs pulse duration, power = 705 mW, fluence = 2.5 J/cm^2, 10 kHz repetition rate, TETA 10 model, Avesta, Moscow, Russia) was focused by a 70 mm lens on the surface of the target through a side wall of the vessel. The thickness of the liquid layer from the entrance glass to the target surface was 2 mm. The ablation vessel was mounted on a platform, which performed one-shot scanning over a 10 × 10 mm area with the two speed-modes: 870 and 3840 mm/sec, which corresponded to the irradiation spot displacement by 0.5 and 2 laser beam diameters, respectively, Fig. 1a. A detailed scheme of a PLAL process is shown in Fig. 1b.

After the generation of colloids, both obtained solutions were investigated by Transmission Electron Microscopy (TEM) using a JEOL JEM-2010 system. TEM images were obtained at 200 keV accelerating voltage. Size distributions of the synthesized Au NPs were obtained by means of the analysis of TEM images by ImageJ software using the circle fit approximation. The final distributions of the 870 mm/sec and 3840 mm/sec regime were based on the obtained measurements and plotted in the Origin software environment. The resulting images were processed, and the particle size distribution was calculated using the ImageJ and Origin program. In the case when the laser beam shifted by half the diameter with the beam speed 870 mm/sec on the target surface, the size of the obtained nanoparticles lay in the narrow range of

1-11 nm with a local maximum of 4 nm. In the case of a laser beam offset by two diameters with the beam speed 3840 mm/sec, the size of the nanoparticles lay in the wide range of 1-40 nm and the distribution was bimodal with two local maxima of 5 and 25 nm.

2.2. Numerical modelling

The simulations were performed using a combined atomistic continuum model, which describes non-equilibrium laser-induced phase transitions at the atomic level via Molecular Dynamics (MD), whereas laser light absorption, fast electron heat conduction, and strong electron-phonon non-equilibrium (developed during the ultrashort laser pulses) are addressed using Two Temperature Model (TTM) [64] in continuum. Such a combined MD-TTM model has been successfully exploited to study ultrashort pulse laser melting and ablation processes [65], nanostructuring of materials [66] and NPs generation in different media [52,67]. Thus, the MD-TTM model has manifested itself as a powerful numerical tool to investigate transient states of matter induced by an ultrashort pulsed laser energy deposition and as a predictive instrument to describe laser-ablative modification of surfaces with predesigned properties. The basics of this model was described in Ref. [68], and its application for NPs generation due to PLAL was extended in our recent works [39,51,52]. The principle of operation of the model is schematically described in Fig. 2. An initial monocrystalline sample of [1,0,0] orientation with the dimensions of 80nm x 80nm x 700nm in X, Y, and Z directions, totally accounting for 175,000,000 atoms, was equilibrated at normal conditions. Assuming the size of laser spot much greater than the lateral size of the modelled volume, we apply periodic boundary conditions (PBC) over X and Y axes and we use transparent for the heat flux non-reflective boundaries conditions (NRB) at the bottom of the MD domain (where laser-generated pressure waves are absorbed), limiting the application of the combined model MD-TTM in Z axis [69,70], meanwhile providing the cooling of the surface region. Atop the metal target, we place a water layer, equilibrated with the target and ending with the NRB boundary at the distance of 500 nm above the metal surface. For a more efficient parallel processing with MPI, we choose the processor geometry of 36 x 36 x 1 cores in X, Y, and Z directions correspondingly. The porous sample was prepared in the assumption of ~25% porosity in the pre-surface volume, as compared to the bulk sample, by the placement of 3 layers of empty voids at positions of 25 nm, 45 nm, and 60 nm below the initial surface with their volumes of 15 nm^3, 20 nm^3, and 10 nm^3, correspondingly. Such a configuration was chosen based on the data presented in [49,50,63] and the voids with vacuum inside were assumed to be formed due to a spallation onset during the prior virtual laser pulse with the same irradiation parameters, but shifted by

half of the spot diameter. Both bulk and porous sample, prepared and equilibrated under the liquid environment, were then irradiated by a single 270 fs laser pulse at the incident fluence of 2.5 J/cm^2. The process of laser energy absorption and the electron heat conduction in porous sample is automatically accounted in 3D by a continuum part of the combined MD-TTM model. Parameters of the interatomic potential, representing gold material (including the description of the electronic subsystem) and water media, are listed in Refs. [60] and [39] correspondingly. It is worth mentioning here that the interatomic potential function for water does not reproduce all its thermophysical properties, but does reproduce well its mechanical properties, which is more important.

The above described MD-TTM method for the simulation of PLAL experiments, except the interatomic potential function parametrization and computational cell geometry, is similar to methods described and used by other theoretical groups [48,49,50,58]. Unlike the previously used model of the electron thermal conductivity in [39,51,52], in this work we use a more advanced approach that takes into account not only dependencies for electron and lattice temperature, but also that of local density of matter, as suggested in Ref. [56]. Moreover, reflectivity, as a function of the electron temperature, was calculated based on data presented in Ref. [71] and accounted for the absorbed fluence value of 545 mJ/cm^2.

Similar to the model described in detail in our previous research [39], the used model does not take into account any chemistry (e.g., oxidation phenomena) and optical non-linearity in liquid media. Also, due to a high computational cost of simulation we limit our modeling to 2.5 ns of the experimental time, when the active process of NPs formation ceases and the effect of periodic boundaries in X and Y direction becomes significant, which can bring certain artificiality into the obtained NPs' characteristics. Because of the same reason, the investigation of NPs formation due to ns pulses, where slower processes like precipitation and growth of NPs due to diffusion of metal atoms in liquid media and coalescency of small clusters can start providing a major input, the model is basically limited to the pulse durations of 100's ps. Nevertheless, the performed in this study simulations clearly isolate the main driving mechanisms of the NPs formation that are responsible for the initial system evolution, which however determines its future dynamics on a larger time scale in general. Here, regarding the effect of porosity on the NPs formation process, we rely on the experimental verification of the theoretical prediction drawn from our modeling and interpretation of the obtained results.

Thus, the suggested above computational approach is aimed at the identification of main effects involved in the NPs formation, and the effect of water media is mainly caused by its mechanical action and thermal energy sink due to vaporization losses. Nevertheless, we believe that the above model can capture the essential processes involved in the NPs formation process due to PLAL and the described approach is an important step forward towards generation of colloidal NPs with predesigned properties.

3. Results and discussion

The results of the simulations can be seen in Fig. 3, where the atomic snapshots of the irradiated targets' evolution are shown for the time of 1000 ps after the pulse. For the case of bulk target, Fig. 3 (a), we observe the large clusters and irregular shape pillars of the molten material developing across the moving metal-water interface as a result of Rayleigh-Taylor instabilities. In contrast, the irradiation of the porous sample, Fig. 3 (b), results in the nucleation of small NPs of spherical shape atop a molten upper part of the metal target, which moves upward with a smaller speed. In the former case, the growing instabilities will eventually decompose to large NPs, while the remaining vapor atoms (in much lower quantities than in the case of the porous target) will nucleate into the NPs of smaller size, Fig. 3 (a). In the latter case, however, the surface of porous sample undergoes a much stronger overheating that results in a stronger evaporation process and the formation of significantly larger quantity of vapor (red atoms). Then, the vapor passes through a stage of a massive nucleation during a subsequent cooling process due to the presence of liquid and significant thermal losses due to its evaporation, leading to the formation ~5-10 nm NPs, Fig 3(b).

A visual analysis of the bulk and porous ablated samples reveals that the spallation mechanism of the material ejection, responsible for the establishment of upward motion of the pre-surface region due to the formation of internal voids [60,62,63], is present in both cases. It is nevertheless more pronounced for the case of the bulk target, that is reflected by a different position of the ablative mass, indicated by white arrowed marks in Fig. 3. Eventually, the relative difference between the height of the ablation plumes in 20% is reached by t = 2,5 ns with the values of 900 nm and 750 nm above the initial position for the bulk and porous samples correspondingly. Thus, for the case of bulk sample irradiation, we reproduce conditions for bimodal NPs size distribution that was registered experimentally [40,43,45] and observed in numerical simulations [39,48,49]. However, despite the fact that we still observe the development of Rayleigh-Taylor instabilities in the case of porous material, its input to the

mechanism of NPs formation of the larger population is insignificant and seems to be suppressed. Therefore, the first visual analysis of both targets' evolution due to PLAL emphasizes the benefit of porous target utilization in the NPs production for variety applications.

In order to perform a more formal analysis of the laser-induced processes in the targets, responsible for the NPs formation, in Fig. 4 we show the lattice temperature and pressure fields in the pre-surface regions of the samples at t = 15 ps, when their maximum values are reached. From the analysis of temperature fields of bulk and porous targets, Fig. 4(a) and 4(b) correspondingly, one can clearly see that the laser-deposited energy in the porous sample does not penetrate to the material as fast and deep as it is in the case of the bulk sample. In general, there are two essential channels of the laser-deposited energy dissipation [53,72]: via the electron-phonon coupling connected with the rate of lattice heating, and the electron heat conduction, connected with the effective heating depth of the irradiated material [73]. Both channels are strong functions of the electronic and lattice temperatures and the local material density [55,56,74]. If, however, the electron-phonon coupling is a smooth function of electronic temperature (gradually decreasing or increasing) [74], the electronic conductivity demonstrates a complex behavior depending on the level of excitation [55,56]. The latter one gives us the possibility to manipulate with the amount of heat dissipated through this channel (the electron-phonon coupling) via varying the laser fluence, and thus to control the amount of heat dissipated through the other channel (the electron thermal conductivity).

The presence of pores in pre-surface layer of the porous target suppresses the laser-deposited energy dissipation via the electron heat conduction channel, increasing therefore its part dissipating through the electron-phonon relaxation. The latter results in a greater lattice temperature elevation in the proximity of the porous sample's surface as compared to the case of the bulk sample. As a result, the lattice temperature reaches its critical value (~6500 K), and a significant part of the material is removed by explosive boiling mechanism [75]. In contrast, the channel of laser-deposited energy dissipation via fast electronic conductivity is active in the case of the bulk sample, which results in the penetration of a significant part of the deposited energy deeper to the sample and the establishment of strong temperature and pressure gradients across a longer spatial scale. When dealing with a short pulse (much shorter than the characteristic electron-phonon equilibration time, ~ 20 ps), the material heating rate exceeds its acoustic (mechanical) relaxation rate, and the conditions of internal stress confinement are developed within 100-200 nm below the surface [76].

If such conditions are realized, the process of material ejection is governed by means of the spallation mechanism, which leads to the establishment of active motion of the metal–liquid interface upwards during PLAL. This can be seen in Fig. 4(c), in which a strong pressure wave resulting from the relaxation of the laser-induced internal stresses propagates to the bulk of material downward. For the porous material, however, any accumulating internal stresses due to the ultrafast laser energy deposition rate instantly relax to the pores, since the acoustic relaxation rate is determined by the characteristic distance between them. This results in a insignificant rise of pressure, Fig. 4(d), as compared to the case of bulk sample, and the development of the metal-liquid interface upward motion due to the suppression of the spallation mechanism (although it is still present). Since the heat flux is limited, the remaining channel of the energy dissipation via the electron-phonon coupling results in high values of the lattice temperature developed on the surface that is similar to the regime of thermal confinement [72].

Thus, one of the most important conclusions of the present work is that for the production of fine population of NPs, one should use the regime of thermal confinement (responsible for the material ejection via the explosive boiling mechanism) rather than the regime of mechanical confinement (responsible for material modification via spallation mechanism), frequently suitable for nanostructuring purposes. The former can be activated by means of increasing of both the pulse duration and the incident fluence [50,51,52], whereas the latter can be triggered by means pulse shortening (at least shorter than the characteristic electron-phonon equilibration time) and working at fluencies just above the threshold of material modification (melting threshold) [53,72]. Finally, both regimes are not well-separated and normally accompany each other. Therefore, the conclusion above is not a “rule of thumb” for an easy isolation of one regime from the other, but there are such irradiation regimes (trending to the above conclusion), when one or the other mechanism of material modification/ejection can be suppressed as compared to the other one.

For the qualitative analysis of size characteristics of NPs formed as a result of PLAL process, we characterize them with the size distribution obtained from the simulations, Fig. 5 (a) and (b), and compare them to the distributions measured in the experiment, Fig. 5 (c) and (d). As one can see, the result of NPs production due to PLAL of bulk sample indicates their multimodal size distribution, Fig. 5(a), with a little contribution from a small (< 10 nm) population of NPs. This situation was already registered and explained in several previous experimental and theoretical works [45,40,43,48,49,39]. In the case of the porous target, however, due to limited

input of the spallation mechanism of material ejection and enhanced heating of the surface layer, Fig. 5(b), the formation of the coarse population of NPs is suppressed, while the fine population have the size within the range of 5-10nm is drastically increased.

Experimentally, the NPs generation in water due to a 270 fs laser pulse at the incident fluence of 2.5 J/cm^2 was measured in a multipulse regime, Fig. 5 (c) demonstrate the resulting NPs size distribution obtained with the scanning speed of 3840 mm/sec, which roughly corresponds to the shift of each new pulse to approximately two diameters the laser spot on the material's surface. Thus, each new laser short ablates fresh surface related to our simulation of the laser pulse interaction with the bulk target, Fig. 3(a). As we can see, the size distribution has a broad character with uncertain mean size. Alternatively, Fig. 5 (d), shows the NPs size distribution obtained with the scanning speed of 870 mm/sec, which roughly corresponds to the shift of each new pulse to approximately half of the laser spot diameter. Thus, each new short ablates the surface, which already has a porosity, predeveloped by the previous pulse due to local fluence being below the spallation threshold. Clearly, this case corresponds to the simulation of laser pulse interaction with the porous target, Fig. 3 (b). The resulting size distribution of NPs has a clear unimodal character with a narrow size dispersion and the mean size of about 4 nm. Thus, the experimental measurements not only confirm our theoretical model, but also constitute a step towards the elaboration of the methodology for the fabrication of NPs with controllable size characteristics.

4. Conclusions

It was found that the regime of PLAL and the final product characteristics are determined by two channels for the laser-deposited energy dissipation, which are governed by the electron-phonon coupling and the electron heat conduction processes. Both channels are strong functions of the electronic temperature. In turn, the characteristic electronic temperature variations range during the pulse is strongly determined by the pulse duration and the absorbed fluence. These connections give us a possibility for the manipulation of size characteristics of formed NPs' via the variation of laser irradiation parameters. In particular, for the production of fine (small size) population of NPs it is important to work in the regime of thermal confinement for the development of preferably higher surface temperature with the subsequent material removal via the explosive boiling mechanism. This mechanism can be achieved at high fluence regime to generate a significant amount of vapor, which leads to the formation of fine NPs population during the nucleation process. Meanwhile, in order to avoid the spallation mechanism of the material ejection and an intensive motion of the metal-liquid interface (with a subsequent

development of the Rayleigh-Taylor instabilities and their fragmentation to large material's fractions) the use of long pulses excludes the internal stresses confinement regime and thus benefits over the short and ultrashort pulses for the production of NPs of fine population in liquids. Due to the model limitations, however, we could not take into account the evolution of NPs' parameters on microsecond time scale, which could bring some corrections to the size characteristics of formed NPs.

While the effect of pulse duration and the absorbed fluence on the NPs formation process in liquids has been recently studied, the applications of different pulse regimes (single pulse or multi-pulse regime), and its connections with different regimes of the laser energy dissipation, is investigated for the first time. Namely, in this study we focused on the qualitative effect of predeveloped porosity at the front edge of the scanning laser spot in the context of generation of NPs with prescribed characteristics. Based on theoretical predictions we describe the mechanism of the presurface porosity generation in the multi-pulse regime of PLAL and address its effect on the NPs' yield. The experimental measurement completely confirmed the suggested theoretical approach and drawn prediction from the obtained simulation results. Although it was not possible to completely suppress or isolate one or another channel for the laser-deposited energy dissipation, one can experimentally tune the regimes of laser irradiation, which can provide the unimodal size distribution of NPs of spherical shape. Considering the scanning geometry, one can achieve the generation of the porous pre-surface layer at the front of the laser spot and obtain the NPs of small and narrow size distribution.

Based on its accuracy and advanced material description, the proposed model can be considered as one of for-front technologies for the prediction of evolution of an excited atomic system at the present. Moreover, the internal built-in models related to laser light absorption, electron heat conduction and electronic properties of material do not limit the MD-TTM approach to a particular choice of material and the computational cell geometry. Thus, with the available description of the material's properties the model can be easily adapted and extended to other metals and liquids. In general, since the effect of the laser-induced stresses on the formation of NPs is suppressed due to presence of porosity, we can expect qualitatively similar results for other metals both noble (Pt, Ag) and transition (Ni, Al). Finally, due to water model representation used in this work, similar results can be obtained with other liquids of similar mechanical properties (spirits, acetone).

Acknowledgements

Research carried out with the financial support of Ministry of Science and Higher Education of Russian Federation (project No 075-15-2021-1347). We also thank Prof. Martin E. Garcia (University of Kassel) and Prof. Baerbel Rethfeld (TU-Kaiserslautern) for fruitful discussions and valuable comments during preparation of this work.

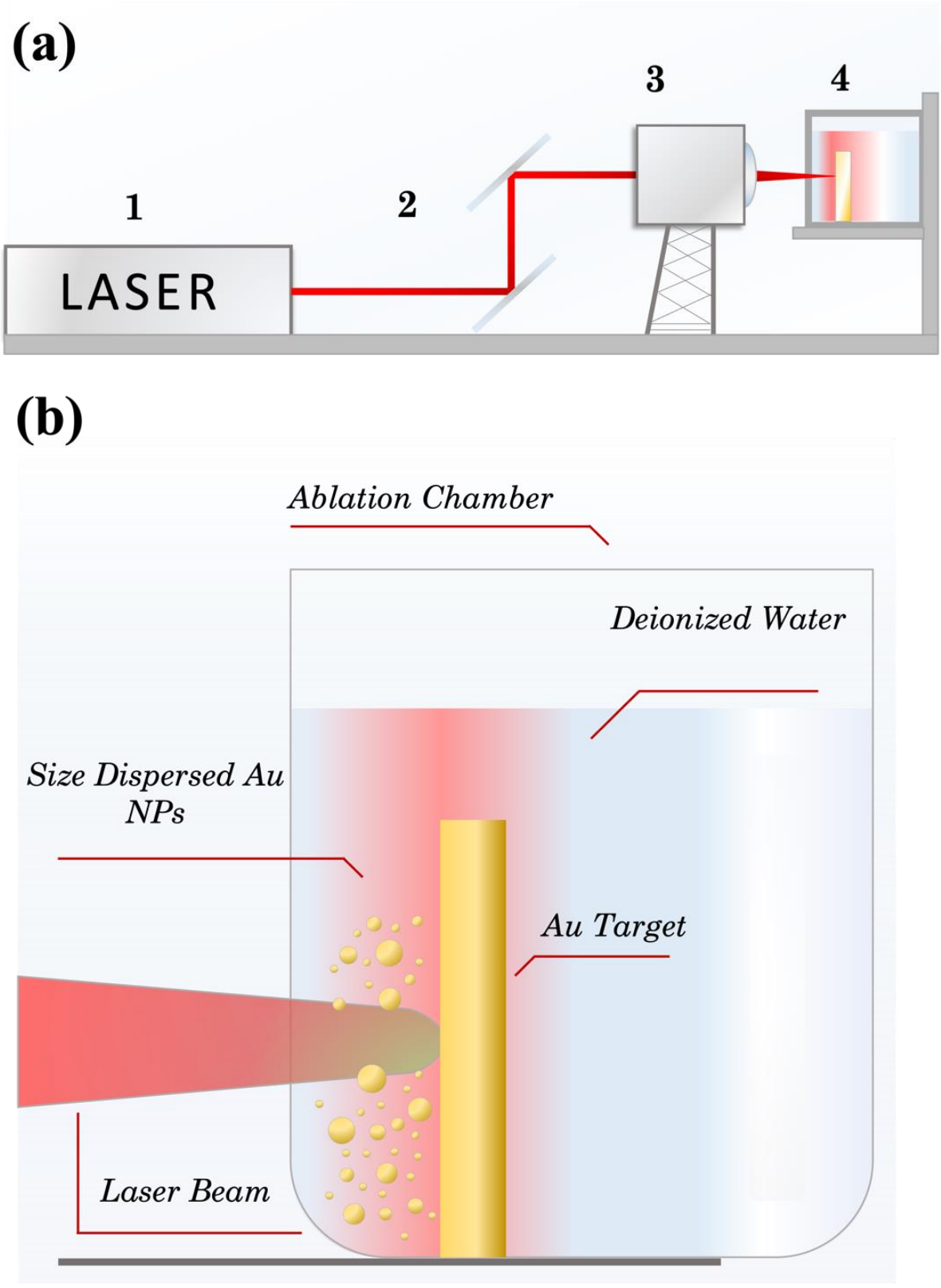

Figure 1: (a) Scheme of the experiment: 1 – femtosecond laser Yb: KGW; 2 – dielectric mirror; 3 – galvanometric scanner (Ateko F-Theta lens with a working field of 70x70 mm, focal length f' = 100 mm); 4 – ablative chamber with a target; and (b) the detailed scheme of PLAL processing for a gold target

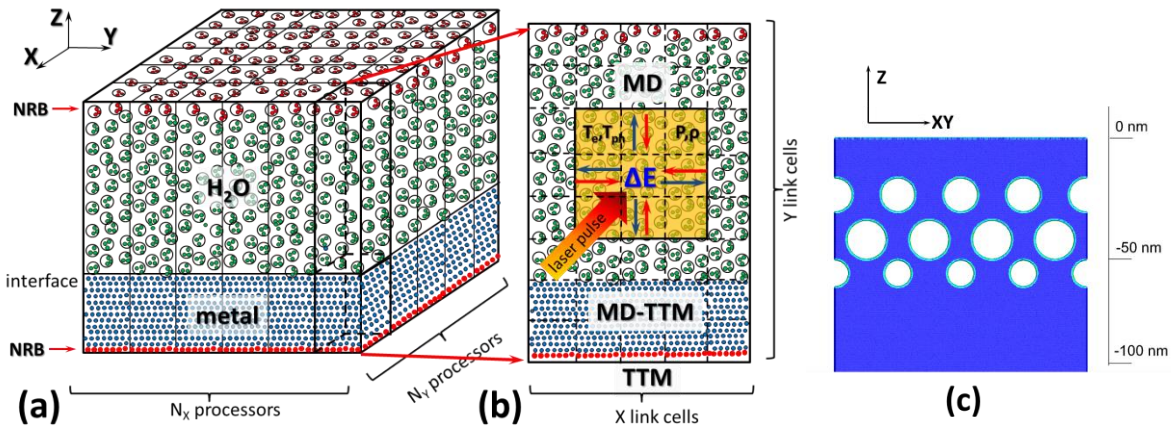

Figure 2: Schematic representation of the combined atomistic-continuum MD-TTM model in parallel multiprocessing regime for large scale simulations of NPs formation due to PLAL (a) and its realization in 3D mesh (b). Surface volume slice in [1,1,0] direction indicating the relative position of the prepared voids (c).

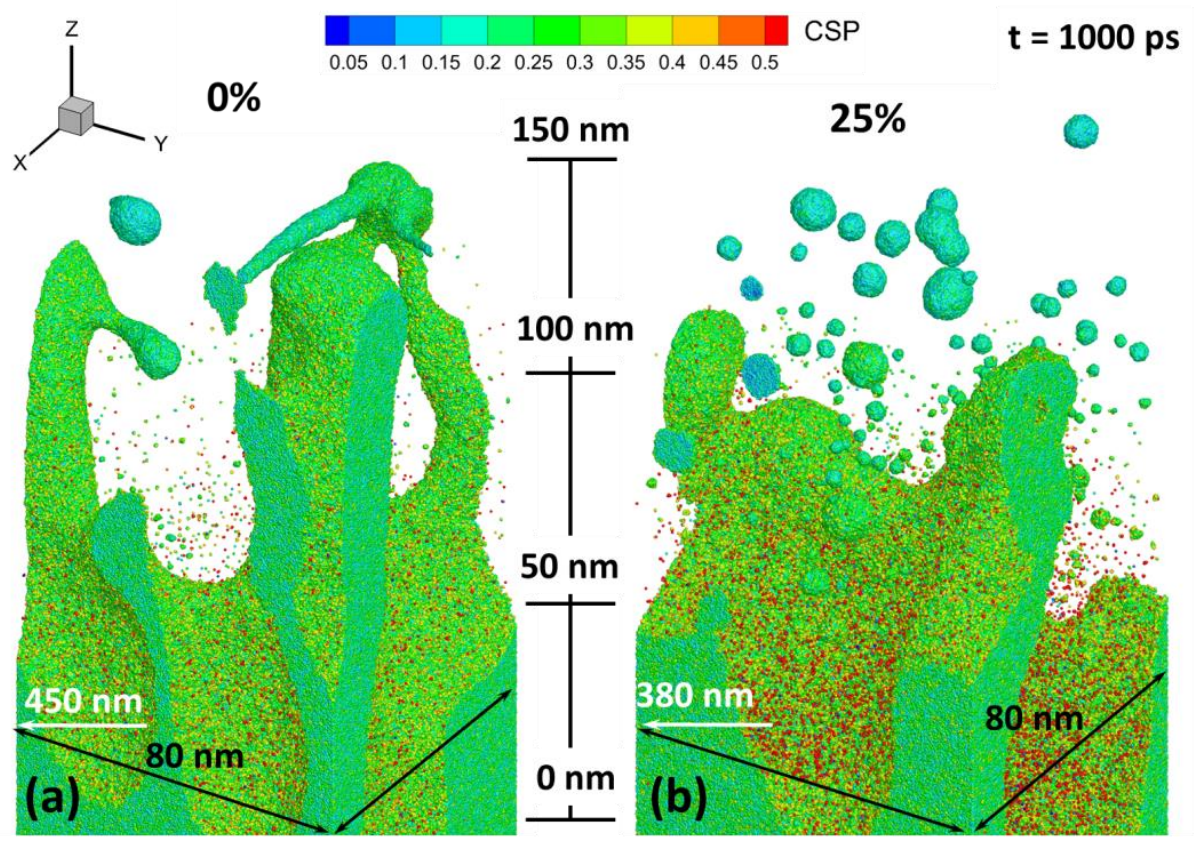

Figure 3: The atomic snapshots of the irradiated target in water at t =1000 ps after the pulse for initially bulk (a) and porous (b) targets. The top 150 nm of the ablating metal target is shown for both cases with the corresponding positions of the ablating surfaces indicated by white arrows. Water atoms are not shown for a better visual analysis. The atoms are colored by Central Symmetry Parameter (CSP) to distinguish a local crystal structure as follows: crystal < 0.08 < defects (dislocations) < 0.11 < liquid < 0.25 < surfaces < 0.50 < vapor (free atoms).

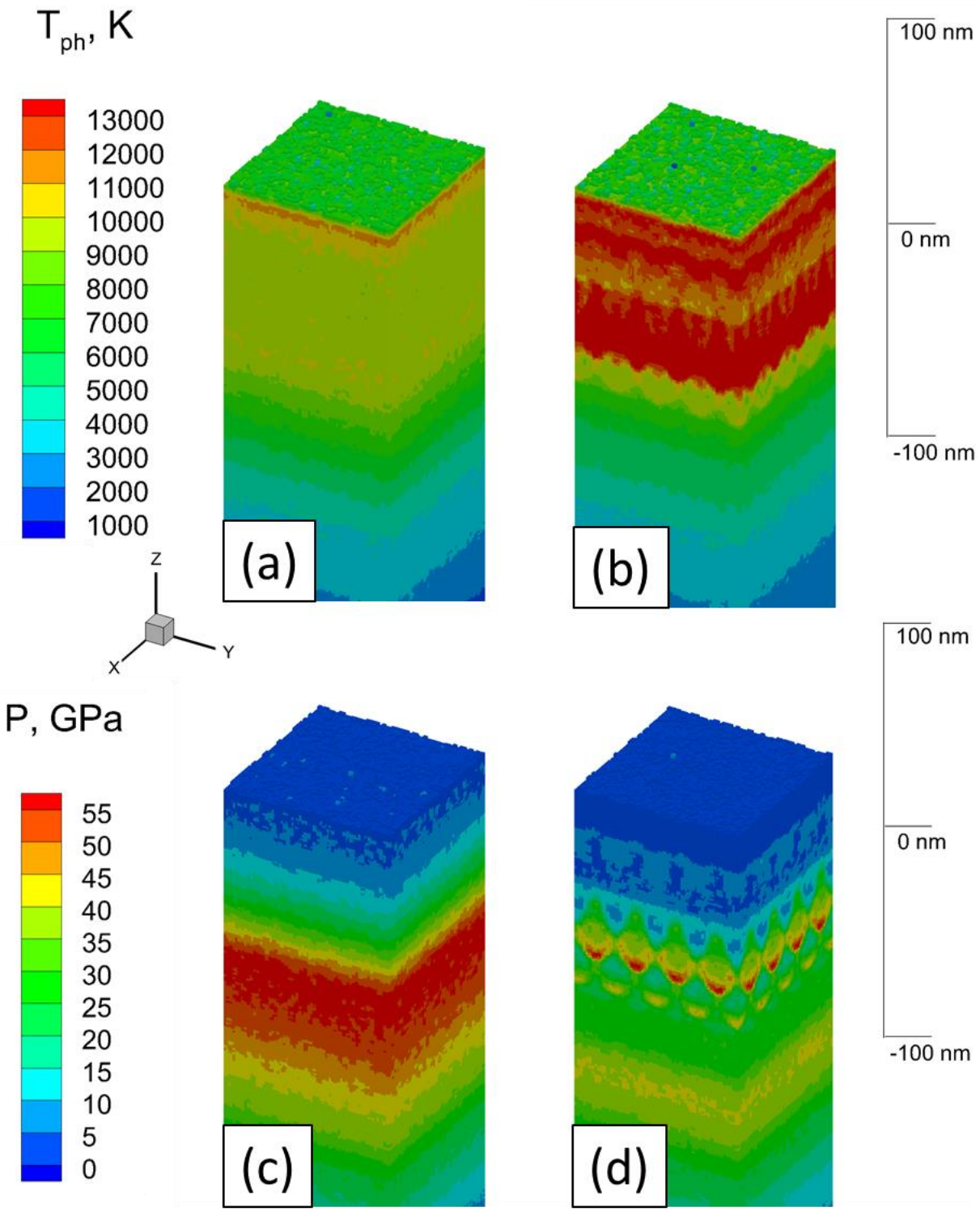

Figure 4: Temperature field in the Au target at t = 15ps after the pulse, shown by color for the bulk (a) and porous (b) targets. Pressure field in the Au target at t = 15ps after the pulse, shown by color for the bulk (c) and porous (d) targets. The liquid above the target is blanked. The level "0 nm" indicates the initial position of the target's surface.

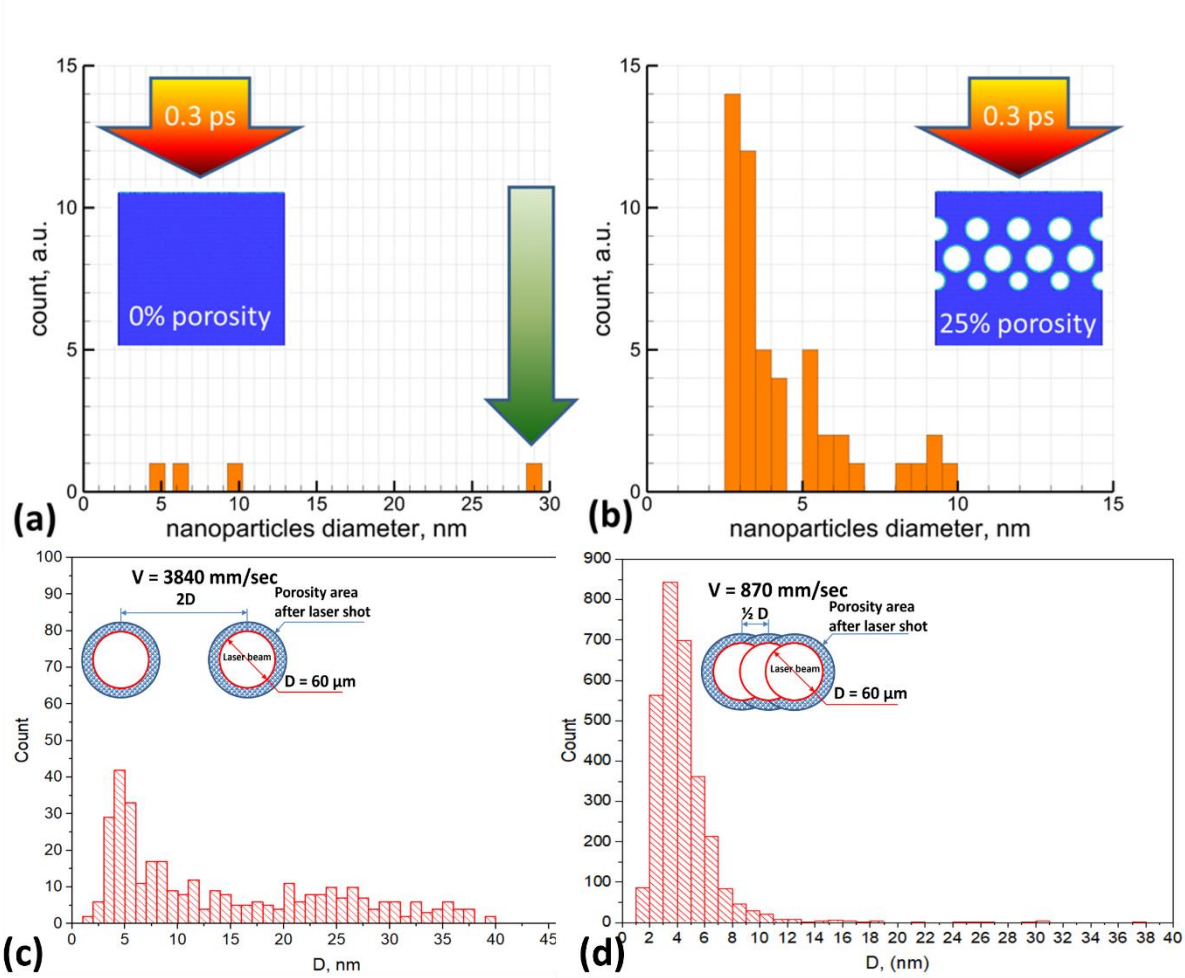

Figure 5: The NPs size distribution due to the PLAL obtained in simulation with a bulk (a) and porous (b) targets. The wide arrow in (a) indicates the region of formation of a coarse (large size) population due to the decomposition of Rayleigh -Taylor instabilities. The NPs smaller of 2nm are not shown for a better visual interpretation. The experimentally measured NPs distribution in a multipulse regime of 270 fs laser pulse interacting with a gold sample at the incident fluence of 2.5 mJ/cm^2 in a scanning regime with the speed of 3840 mm/sec, corresponding to the shift of two laser spot diameter (c), and 870 mm/sec, corresponding to the shift of a half laser spot diameter (d).

REFERENCES

[1] A.C. Anselmo, S. Mitragotri, "Nanoparticles in the clinic", *Bioeng. Transl. Med.* **1**, 10–29 (2016).

[2] G. Chen, I. Roy, C. Yang, P.N. Prasad, "Nanochemistry and nanomedicine for nanoparticle-based diagnostics and therapy", *Chem. Rev.* 116, 2826–2885 (2016).

[3] Xuan Yang, Miaoxin Yang, Bo Pang, Madeline Vara, and Younan Xia, Gold Nanomaterials at Work in Biomedicine, *Chem. Rev.* **115**, 19, 10410–10488 (2015).

[4] E.C. Wang and A.Z. Wang, "Nanoparticles and their Applications in Cell and Molecular Biology", *Integr. Biol. (Camb).* **6**, 9–26 (2014).

[5] Yu-Feng Li and Chunying Chen, "Fate and Toxicity of Metallic and Metal-Containing Nanoparticles for Biomedical Applications", *Small* **7**, 2965–2980 (2011).

[6] M. Yu, and J. Zheng, "Clearance Pathways and Tumor Targeting of Imaging Nanoparticles", *ACS Nano* **9**, 6655–6674 (2015).

[7] Karrina McNamara and Syed A. M. Tofail, "Nanosystems: the use of nanoalloys, metallic, bimetallic, and magnetic nanoparticles in biomedical applications", *Phys. Chem. Chem. Phys.* **17**, 27981-27995 (2015).

[8] Minho Kim, Jung-Hoon Lee, and Jwa-Min Nam, "Plasmonic Photothermal Nanoparticles for Biomedical Applications", *Adv. Sci.* **6**, 1900471 (2019).

[9] E.C. Dreaden, A.M. Alkilany, X. Huang, C.J. Murphy, M.A. El-Sayed, "The golden age: gold nanoparticles for biomedicine", *Chemical Society Reviews* **41**, 2740-2779 (2012).

[10] A.V. Kabashin, P. Delaporte, A. Pereira, D. Grojo, R. Torres, T. Sarnet, M. Sentis, Nanofabrication with pulsed lasers, Nanoscale research letters, 5 (2010) 454-463.

[11] D. Zhang, B. Gokce, S. Barcikowski, Laser synthesis and processing of colloids: fundamentals and applications, Chemical reviews, 117 (2017) 3990-4103.

[12] D.B. Geohegan, A.A. Puretzky, G. Duscher, S.J. Pennycook, Photoluminescence from gas-suspended SiO x nanoparticles synthesized by laser ablation, Applied Physics Letters, 73 (1998) 438-440.

[13] T.E. Itina, K. Gouriet, L.V. Zhigilei, S. Noël, J. Hermann, M. Sentis, Mechanisms of small clusters production by short and ultra-short laser ablation, Applied Surface Science, 253 (2007) 7656-7661.

[14] L. Patrone, D. Nelson, V. Safarov, M. Sentis, W. Marine, S. Giorgio, Photoluminescence of silicon nanoclusters with reduced size dispersion produced by laser ablation, Journal of Applied Physics, 87 (2000) 3829-3837.

[15] Y. Yamada, T. Orii, I. Umezu, S.T.S. Takeyama, T.Y.T. Yoshida, Optical properties of silicon nanocrystallites prepared by excimer laser ablation in inert gas, Japanese journal of applied physics, 35 (1996) 1361.

[16] A.V. Kabashin, M. Meunier, R. Leonelli, Photoluminescence characterization of Si-based nanostructured films produced by pulsed laser ablation, Journal of Vacuum Science & Technology B: Microelectronics and Nanometer Structures Processing, Measurement, and Phenomena, 19 (2001) 2217-2222.

[17] A.V. Kabashin, M. Meunier, Laser-induced treatment of silicon in air and formation of Si/SiOx photoluminescent nanostructured layers, Materials Science and Engineering: B, 101 (2003) 60-64.

[18] A. Fojtik, A. Henglein, Laser ablation of films and suspended particles in a solvent: formation of cluster and colloid solutions, BERICHTE-BUNSENGESELLSCHAFT FUR PHYSIKALISCHE CHEMIE, 97 (1993) 252-252.

[19] M.S. Sibbald, G. Chumanov, T.M. Cotton, Reduction of cytochrome c by halide-modified, laser-ablated silver colloids, The Journal of Physical Chemistry, 100 (1996) 4672-4678.

[20] F. Mafuné, J.-y. Kohno, Y. Takeda, T. Kondow, Full physical preparation of size-selected gold nanoparticles in solution: laser ablation and laser-induced size control, The Journal of Physical Chemistry B, 106 (2002) 7575-7577.

[21] A.V. Kabashin, M. Meunier, Synthesis of colloidal nanoparticles during femtosecond laser ablation of gold in water, Journal of Applied Physics, 94 (2003) 7941-7943.

[22] V. Amendola, S. Scaramuzza, L. Litti, M. Meneghetti, G. Zuccolotto, A. Rosato, E. Nicolato, P. Marzola, G. Fracasso, C. Anselmi, Magneto-plasmonic Au-Fe alloy nanoparticles designed for multimodal SERS-MRI-CT imaging, Small, 10 (2014) 2476-2486.

[23] A.V. Kabashin, V.Y. Timoshenko, What theranostic applications could ultrapure laser-synthesized Si nanoparticles have in cancer?, in, Future Medicine, 2016, pp. 2247-2250.

[24] V. Petriev, V. Tischenko, A. Mikhailovskaya, A. Popov, G. Tselikov, I. Zelepukin, S. Deyev, A. Kaprin, S. Ivanov, V.Y. Timoshenko, Nuclear nanomedicine using Si nanoparticles as safe and effective carriers of 188Re radionuclide for cancer therapy, Scientific reports, 9 (2019) 2017.

[25] A.V. Kabashin, A. Singh, M.T. Swihart, I.N. Zavestovskaya, P.N. Prasad, Laser-processed nanosilicon: A multifunctional nanomaterial for energy and healthcare, ACS nano, 13 (2019) 9841-9867.

[26] J. Zhang, M. Chaker, D. Ma, Pulsed laser ablation based synthesis of colloidal metal nanoparticles for catalytic applications, Journal of colloid and interface science, 489 (2017) 138-149.

[27] S. Hebie, Y. Holade, K. Maximova, M. Sentis, P. Delaporte, K.B. Kokoh, T.W. Napporn, A.V. Kabashin, Advanced electrocatalysts on the basis of bare Au nanomaterials for biofuel cell applications, ACS Catalysis, 5 (2015) 6489-6496.

[28] S. Reichenberger, G. Marzun, M. Muhler, S. Barcikowski, Perspective of surfactant-free colloidal nanoparticles in heterogeneous catalysis, ChemCatChem, 11 (2019) 4489-4518.

[29] R.C. Forsythe, C.P. Cox, M.K. Wilsey, A.M. Müller, Pulsed Laser in Liquids Made Nanomaterials for Catalysis, Chemical Reviews, 121 (2021) 7568-7637.

[30] C. Petridis, K. Savva, E. Kymakis, E. Stratakis, Laser generated nanoparticles based photovoltaics, Journal of Colloid and Interface Science, 489 (2017) 28-37.

[31] A.V. Kabashin, M. Meunier, Femtosecond laser ablation in aqueous solutions: a novel method to synthesize non-toxic metal colloids with controllable size, in: Journal of Physics: Conference Series, IOP Publishing, 2007, pp. 354.

[32] J.-P. Sylvestre, A.V. Kabashin, E. Sacher, M. Meunier, Femtosecond laser ablation of gold in water: influence of the laser-produced plasma on the nanoparticle size distribution, Applied Physics A, 80 (2005) 753-758.

[33] M. Kögler, Y.V. Ryabchikov, S. Uusitalo, A. Popov, A. Popov, G. Tselikov, A.L. Välimaa, A. Al-Kattan, J. Hiltunen, R. Laitinen, Bare laser-synthesized Au-based nanoparticles as nondisturbing surface-enhanced Raman scattering probes for bacteria identification, Journal of biophotonics, 11 (2018) e201700225.

[34] A.A. Popov, G. Tselikov, N. Dumas, C. Berard, K. Metwally, N. Jones, A. Al-Kattan, B. Larrat, D. Braguer, S. Mensah, Laser-synthesized TiN nanoparticles as promising plasmonic alternative for biomedical applications, Scientific reports, 9 (2019) 1194.

[35] J.C. Bulmahn, G. Tikhonowski, A.A. Popov, A. Kuzmin, S.M. Klimentov, A.V. Kabashin, P.N. Prasad, Laser-ablative synthesis of stable aqueous solutions of elemental bismuth nanoparticles for multimodal theranostic applications, Nanomaterials, 10 (2020) 1463.

[36] A.Y. Kharin, V.V. Lysenko, A. Rogov, Y.V. Ryabchikov, A. Geloen, I. Tishchenko, O. Marty, P.G. Sennikov, R.A. Kornev, I.N. Zavestovskaya, Bi-Modal Nonlinear Optical Contrast from Si Nanoparticles for Cancer Theranostics, Advanced Optical Materials, 7 (2019) 1801728.

[37] V. Oleshchenko, A.Y. Kharin, A. Alykova, O. Karpukhina, N. Karpov, A. Popov, V. Bezotosnyi, S. Klimentov, I. Zavestovskaya, A. Kabashin, Localized infrared radiation-induced hyperthermia sensitized by laser-ablated silicon nanoparticles for phototherapy applications, Applied Surface Science, 516 (2020) 145661.

[38] G.I. Tselikov, G.A. Ermolaev, A.A. Popov, G.V. Tikhonowski, D.A. Panova, A.S. Taradin, A.A. Vyshnevyy, A.V. Syuy, S.M. Klimentov, S.M. Novikov, Transition metal dichalcogenide nanospheres for high-refractive-index nanophotonics and biomedical theranostics, Proceedings of the National Academy of Sciences, 119 (2022) e2208830119.

[39] D.S. Ivanov, Th. Izgin, A.N., V.P. Veiko, B. Rethfeld, Y.I. Dombrovska, M.E. Garcia, I.N. Zavestovskaya, S.M. Klimentov, A.V. Kabashin, “Numerical Investigation of Ultrashort

Laser-Ablative Synthesis of Metal Nanoparticles in Liquids Using Atomistic-Continuum Model", *Molecules* **25**, 67 (2020).

[40] J. Bonse, S. Baudach, J. Krüger, W. Kautek, M. Lenzner, "Femtosecond Laser Ablation of Silicon−Modification Thresholds and Morphology", *Appl. Phys. A: Mater. Sci. Process*. **74**, 19−25 (2002).

[41] H. Liu, F. Chen, X. Wang, Q. Yang, H. Bian, J. Si, X. Hou, Influence of liquid environments on femtosecond laser ablation of silicon, Thin Solid Films, 518 (2010) 5188-5194.

[42] W.T. Nichols, T. Sasaki, N. Koshizaki, Laser ablation of a platinum target in water. I. Ablation mechanisms, Journal of Applied Physics, 100 (2006) 114912.

[43] G. Marzun, J. Nakamura, X. Zhang, S. Barcikowski, P. Wagener, Size control and supporting of palladium nanoparticles made by laser ablation in saline solution as a facile route to heterogeneous catalysts, Applied Surface Science, 348 (2015) 75-84.

[44] L. Gamrad, C. Rehbock, J. Krawinkel, B. Tumursukh, A. Heisterkamp, S. Barcikowski, Charge balancing of model gold-nanoparticle-peptide conjugates controlled by the peptide's net charge and the ligand to nanoparticle ratio, The Journal of Physical Chemistry C, 118 (2014) 10302-10313.

[45] S. Barcikowski, A. Menéndez-Manjón, B. Chichkov, M. Brikas, and G. Račiukaitis, "Generation of nanoparticle colloids by picosecond and femtosecond laser ablations in liquid flow", *Appl. Phys. Lett.* **91**, 083113 (2007).

[46] J. Noack, A. Vogel, Laser-induced plasma formation in water at nanosecond to femtosecond time scales: calculation of thresholds, absorption coefficients, and energy density, IEEE journal of quantum electronics, 35 (1999) 1156-1167.

[47] Y. Andreeva, N. Sharma, A. Rudenko, J. Mikhailova, M. Sergeev, V.P. Veiko, F. Vocanson, Y. Lefkir, N. Destouches, and T.E. Itina, "Insights into Ultrashort Laser-Driven Au:TiO2 Nanocomposite Formation", *J. Phys. Chem. C* **124**, 10209–10219 (2020).

[48] C.-Y. Shih, R. Streubel, J. Heberle, A. Letzel, N.V. Shugaev, C. Wu, M. Schmidt, B. Gökce, S. Barcikowski, L.V. Zhigilei, "Two mechanisms of nanoparticle generation in picosecond laser ablation in liquids: the origin of the bimodal size distribution", *Nanoscale* **10**,

6900-6910 (2018).

[49] Ch.-Yu Shih, M.V. Shugaev, Ch. Wu, and L.V. Zhigilei, "Generation of Subsurface Voids, Incubation Effect, and Formation of Nanoparticles in Short Pulse Laser Interactions with Bulk Metal Targets in Liquid: Molecular Dynamics Study", *J. Phys. Chem. C* **121**, 16549−16567 (2017).

[50] C.-Y. Shih, M. V. Shugaev, C. Wu, and L. V. Zhigilei, The effect of pulse duration on nanoparticle generation in pulsed laser ablation in liquids: Insights from large-scale atomistic simulations, *Phys. Chem. Chem. Phys.* **22**, 7077-7099 (2020).

[51] K. Zhang, D.S. Ivanov, R.A. Ganeev, G.S. Boltaev, P.S. Krishnendu, S.C. Singh, M.E. Garcia, I.N. Zavestovskaya and Ch. Guo, "Pulse Duration and Wavelength Effects of Laser Ablation on the Oxidation, Hydrolysis, and Aging of Aluminum Nanoparticles in Water", *Nanomaterials* ***9***, 767 (2019).

[52] M. Iqbal, S.A. Khan, D.S. Ivanov, R.A. Ganeev, V.V. Kim, G.S. Boltaev, N.A. Abbasi, S. Shaju, M.E. Garcia, B. Rethfeld and A.S. Alnaser, "The mechanism of laser assisted generation of aluminum nanoparticles, their wettability and nonlinearity properties", *Appl Sur Sci* **527**, 146702 (2020).

[53] D.S. Ivanov, V.P. Lipp, V.P. Veiko, E. Jakovlev, B. Rethfeld, and M.E. Garcia, "Molecular Dynamics Study of the Short Laser Pulse Ablation: Quality and Efficiency in Production", *Appl. Phys. A* **117**, 2133 (2014).

[54] D.S. Ivanov, P.N. Terekhin, S.I. Kudryashov, S.M. Klimentov, A.V. Kabashin, M.E. Garcia, B. Rethfeld, I.N. Zavestovskaya, The atomistic perspective of nanoscale laser ablation, in: Ultrafast Laser Nanostructuring: The Pursuit of Extreme Scales, Springer, 2023, pp. 65-137.

[55] S. I. Anisimov and B. Rethfeld, "On the theory of ultrashort laser pulse interaction with a metal", *Proc. SPIE Int. Soc. Opt. Eng.* **3093**, 192 (1997).

[56] Yu.V. Petrov, N.A. Inogamov, S.I. Anisimov, K.P. Migdal, V.A. Khokhlov, and K.V. Khishchenko, "Thermal conductivity of condensed gold in states with the strongly excited electron subsystem", *Journal of Physics: Conference Series* **653**, 012087 (2015).

[57] C.-Y. Shih, C. Wu, M.V. Shugaev, and L.V. Zhigilei, "Atomistic modeling of nanoparticle generation in short pulse laser ablation of thin metal films in water", *J. Colloid Interface Sci.* **489**, 3-17 (2017).

[58] N.A. Inogamov, V.A. Khokhlov, Yu.V. Petrov, V.V. Zhakhovsky, "Hydrodynamic and molecular-dynamics modeling of laser ablation in liquid: from surface melting till bubble formation", *Optical and Quantum Electronics* **52**, 63 (2020).

[59] K. W. Kolasinski, M. C. Gupta, and L. V. Zhigilei, "Plume and nanoparticle formation during laser ablation", Encyclopedia of Interfacial Chemistry: Surface Science and Electrochemistry (Elsevier, 2018), pp. 594-603.

[60] D.S. Ivanov, V.P. Lipp, A. Blumenstein, V.P. Veiko, E.B. Yakovlev, V.V. Roddatis, M.E. Garcia, B. Rethfeld, J. Ihlemann, and P. Simon, "Experimental and Theoretical Investigation of Periodic Nanostructuring of Au with UV Laser Near the Ablation Threshold", *Phys. Rev. Appl.* **4**, 064006 (2015).

[61] C. Wu, M. S. Christensen, J.-M. Savolainen, P. Balling, and L. V. Zhigilei, "Generation of sub-surface voids and a nanocrystalline surface layer in femtosecond laser irradiation of a single crystal Ag target*", Phys. Rev. B* **91**, 035413 (2015).

[62] C. Wu and L. V. Zhigilei, "Microscopic mechanisms of laser spallation and ablation of metal targets from large-scale molecular dynamics simulations", *Appl. Phys. A* **114**, 11-32 (2014).

[63] D.S. Ivanov, A. Blumenstein, J. Ihlemann, P. Simon, M.E. Garcia, and B. Rethfeld, "Molecular Dynamics Modeling of Periodic Nanostructuring of Metals with a Short UV Laser Pulse under Spatial Confinement by a Water Layer", *Appl. Phys. A* **123**, 744 (2017).

[64] S. I. Anisimov, B. L. Kapeliovich, and T. L. Perel'man, Electron emission from metal surfaces exposed to ultrashort laser pulses, *Sov. Phys. JETP* **39**, 375-377 (1974).

[65] D.S. Ivanov, V.P. Lipp, B. Rethfeld, and M.E. Garcia, "Molecular-dynamics study of the mechanism of short-pulse laser ablation of single-crystal and polycrystalline metallic targets", *J. Opt. Technol*. **81**, 250 (2014).

[66] A. Blumenstein, M.E. Garcia, B. Rethfeld, P. Simon, J. Ihlemann, D.S. Ivanov, "Formation of periodic nano ridge patterns by ultrashort UV laser irradiation of gold", Nanomaterials **10**, 1998 (2020).

[67] M. Venkatesh, R.A. Ganeev, D.S. Ivanov, G.S. Boltaev, V.V. Kim, J. Liang, A.A. Samokhvalov, A.V. Kabashin, S.M. Klimentov, M.E. Garcia and Chunlei Guo, "High-Order Harmonic Generation in Au Nanoparticle-Contained Plasmas", *Nanomaterials* **10**, 234 (2020).

[68] D.S. Ivanov and L.V. Zhigilei, "Combined Atomistic-Continuum Modelling of Short-Pulse Laser Melting and Disintegration of Metal Films", *Phys. Rev. B* **68**, 064114 (2003).

[69] C. Schäfer, H.M. Urbassek, L.V. Zhigilei, and B.J. Garrison, "Pressure-transmitting boundary conditions for molecular dynamics simulations", *Comp. Mater. Sci.* **24**, 421 (2002).

[70] D.S. Ivanov, A.I. Kuznetsov, V.P. Lipp, B. Rethfeld, B.N. Chichkov, M.E. Garcia, W. Schulz, "Short laser pulse surface nanostructuring on thin metal films: direct comparison of molecular dynamics modeling and experiment", *Appl. Phys. A* **111**, 675 (2013).

[71] A. Blumenstein, E.S. Zijlstra, D.S. Ivanov, S.T. Weber, T. Zier, F. Kleinwort, B. Rethfeld, J. Ihlemann, P. Simon, and M.E. Garcia, "Transient Optics of Gold During Laser Irradiation: From First Principles to Experiment", *Phys. Rev. B* **101**, 165140 (2020).

[72] D.S. Ivanov and B.C. Rethfeld, "The Effect of Pulse Duration on the Character of Laser Heating: Photo-Mechanical vs. Photo-Thermal Damage of Metal Targets", *Appl. Surf. Sci.* **255**, 9724 (2009).

[73] S.-S.Wellershoff, J. Hohlfeld, J. Güdde, E. Matthias, "The role of electron–phonon coupling in femtosecond laser damage of metals", *Appl. Phys. A* **69** [Suppl.], S99–S107 (1999).

[74] Z. Lin, L.V. Zhigilei, and V. Celli, "Electron-phonon coupling and electron heat capacity of metals under conditions of strong electron-phonon nonequilibrium", *Phys. Rev. B* **77**, 075133 (2008).

[75] L.V. Zhigilei, Z. Lin, and D.S. Ivanov, "Atomistic Modeling of Short Pulse Laser Ablation of Metals: Connections Between Melting, Spallation, and Phase Explosion", *J. Chem. Phys.* **113**, 11892 (2009).

[76] L. V. Zhigilei and B. J. Garrison, “Microscopic Mechanisms of Laser Ablation of Organic Solids in the Thermal and Stress Confinement Irradiation Regimes”, *J. Appl. Phys.* **88**, 1281-1298 (2000)